# Domain decomposition deep energy method for phase field analysis in brittle fracture

## A. Chakraborty[1], C. Anitescu[2], S. Goswami[3], X. Zhuang[1] and T. Rabczuk[2]

**[1]Leibniz Unversität Hannover**
**Hannover, Germany**
**[2]Bauhaus Universität Weimar**
**Weimar, Germany**
**[3]Brown University**
**Providence, Rhode Island, United States**

## Abstract

Machine learning techniques have been increasingly used for modeling of engineering problems. In particular, physics informed neural networks (PINNs) have been shown to be a promising approach for discretizing and solving partial differential equations. However, PINNs are best suited for smooth function approximations and have some difficulties dealing with discontinuities and rapidly changing gradients in the solution. Here, we propose a framework for the simulation of nucleation and propagation of cracks under brittle fracture using a subdomain-based phase-field approach. By subdividing the domain into smaller regions and considering an energy minimization formulation, the discontinuous displacements and singular stress fields can be more accurately represented compared to the residual-based formulation.

**Keywords:** domain decomposition, deep energy method, phase field, brittle fracture, energy minimization, physics informed neural networks, artificial neural network, crack propagation

# 1　Introduction

In recent years, scientific machine learning has emerged as an essential tool to address domain specific challenges in computational mechanics and extract insights from scientific datasets and governing partial differential equations (PDEs) through innovative methodological solutions. The theory of employing a neural networks to solve an initial and a boundary value problem defined by a PDE was proposed as early as 1990's [12, 11]. However, this discovery remained theoretical due to the requirement of enormous compute power. The latest resurrection of neural networks — the deep-learning revolution — is the direct outcome of the modern GPUs that has turned the one-layer networks of the 1960s and the two- to three-layer networks of the 1980s into the 10–, 15–, and even 50–layer networks of today. The advent of physics-informed neural networks (PINNs) [16] served as the catalyst for this revolution for computational mechanics engineers, where the hyperparameters of the DNN are optimized by minimizing the residual of the governing PDE, ensuring that the outputs of the network will necessarily satisfy the physics of the problem. Shortly thereafter, a variant of PINNs, the deep energy method [17], was proposed to solve the governing PDE in its weak form. In [17], the authors showed that for approximating the growth of fracture and to obtain the crack path, it is necessary to use the energy minimization form since fracture is an energy-driven phenomenon.

Fracture modeling is a computationally expensive phenomenon as it demands a very fine mesh to resolve the damage region. To design a computationally efficient approach, the same group also proposed an adaptive refinement scheme within the framework of the deep energy method to locally refine the domain along the path of the growth of the crack [10]. To that end, another promising alternative can be the integration of domain decomposition methods with the energy minimization framework. The basic idea behind domain decomposition technique is to divide the global domain into subdomains that can be solved independently and then reconnected by interface conditions. These approaches are naturally applicable to the solution of large-scale problems; their goal is to significantly increase the computational efficiency of simulations.

The developed framework employs phase field modeling approach, a popular continuous fracture modeling technique. The neural networks are trained on the governing coupled PDE (variational form) of the phase field approach to encode the vector valued elastic field and the scalar valued phase field based on the initial crack location, material properties and the characteristic width of the crack. One significant advantage of the proposed variational energy formulation is that it requires derivatives one order lower than the conventional residual minimization approach, which results in better computational efficiency. Additionally, we use Gauss quadrature points to evaluate the integrals, over a domain. To begin with, the computational domain is divided into a number of elements and then, the quadrature points are generated within each element, for an efficient integration of non-smooth functions like fracture.

# 2 Methods

## 2.1 Phase-field based fracture modelling

In this section, we briefly put forth the phase field formulation for brittle fracture analysis. The integration of two fields, the vector-valued elastic field and the scalar-valued phase field, is required to model fracture using the phase field approach. While crack nucleation may be influenced by stress, crack propagation necessitates an increase in the fracture energy or surface energy of a solid, $\Psi_c$ [1]. As a result, the energy criteria is used in the phase field approach to analyse the growth of fracture.

Let us begin with the linear elastic problem on an arbitrary body, $\Omega$, with external boundary $\partial\Omega$. The displacement at each material point $\boldsymbol{x}$ is denoted by $\boldsymbol{u}(\boldsymbol{x})$. In addition, we assume a small strain tensor, $\boldsymbol{\epsilon}$ at each material point defined as,

$$\boldsymbol{\epsilon}(\boldsymbol{u}) = \frac{1}{2}\left(\nabla\boldsymbol{u} + \nabla\boldsymbol{u}^T\right). \tag{1}$$

The displacement field satisfies the Dirichlet and Neumann boundary conditions. Considering the material is isotropic and is linearly elastic, the stored elastic energy, $\Psi_c$ at any material point in the body is described by the energy density function, $\Psi_0(\boldsymbol{\epsilon})$ as:

$$\Psi_0(\boldsymbol{\epsilon}) = \frac{1}{2}\lambda\text{tr}(\boldsymbol{\epsilon})^2 + \mu\text{tr}(\boldsymbol{\epsilon}^2), \tag{2}$$

where $\text{tr}(\cdot)$ denotes the trace of the strain tensor and $\lambda$ and $\mu$ are the Lamé constants. The Cauchy stress tensor, $\boldsymbol{\sigma}$, at any material point on the domain $\Omega$ can be computed as:

$$\boldsymbol{\sigma} = \partial_{\boldsymbol{\epsilon}}\Psi_0(\boldsymbol{\epsilon}) = \lambda\text{tr}(\boldsymbol{\epsilon})\boldsymbol{I} + 2\mu\boldsymbol{\epsilon}. \tag{3}$$

The momentum-balance equation for the elastic field, considering an isotropic solid, can be written as:

$$\begin{aligned}
\nabla \cdot \boldsymbol{\sigma} &= \boldsymbol{f}(\boldsymbol{x}) && \text{in } \Omega, \\
\boldsymbol{u} &= \overline{\boldsymbol{u}} && \text{on } \partial\Omega_D, \\
\boldsymbol{\sigma} \cdot n &= \boldsymbol{t}_N && \text{on } \partial\Omega_N,
\end{aligned} \tag{4}$$

where the Dirichlet and Neumann boundaries are represented by $\partial\Omega_D$ and $\partial\Omega_N$, respectively, $\boldsymbol{t}_N$ is the prescribed boundary force and $\overline{\boldsymbol{u}}$ is the prescribed displacement. The stored internal potential energy of the body, for homogeneous Neumann boundary conditions, is given by:

$$\Psi_{int}(\boldsymbol{u}) = \int_{\Omega} \Psi_0(\boldsymbol{\epsilon})\, d\boldsymbol{x}, \tag{5}$$

and the external energy is given by,

$$\Psi_{ext}(u) = \int_{\Omega} \boldsymbol{f} \cdot \boldsymbol{u}\, d\boldsymbol{x} + \int_{\partial\Omega_N} \boldsymbol{t}_N \cdot \boldsymbol{u}\, d\gamma, \tag{6}$$

where $\boldsymbol{f}$ is the body force.

The equilibrium equation for the elastic field for an isotropic model, considering the evolution of crack, involves the degradation of the stiffness of the material around the area of the crack by penalizing the Cauchy stress tensor, $\boldsymbol{\sigma}$ with a monotonically decreasing stress-degradation function, $g(\phi)$. A common form of the stress-degradation function in the literature is [15]

$$g(\phi) = (1 - \phi)^2.$$

With evolving damage, only the tensile component of the principal stress degrades while the compressive component remains invariant [14]. Therefore, in order to prevent the growth of crack inside regions under compression, a tension-compression split of $\Psi_0(\boldsymbol{\epsilon})$ is considered. With evolving damage, $g(\phi)$ is applied only to the tensile component of the principal strain. Consequently, due to the growth of fracture, the anisotropic constitutive assumption for the degradation of the elastic strain energy, can be stated as:

$$\Psi_e(\boldsymbol{\epsilon}) := g(\phi)\Psi_0^+(\boldsymbol{\epsilon}) + \Psi_0^-(\boldsymbol{\epsilon}), \tag{7}$$

where $\Psi_0^+(\boldsymbol{\epsilon})$ and $\Psi_0^-(\boldsymbol{\epsilon})$ denote the strain energies computed from the positive and negative components of the principal strains, respectively.

The governing equation for the phase-field is written as [2, 6]:

$$\frac{G_c}{l_0}\phi - G_c l_0 \nabla^2 \phi = -g'(\phi)\mathcal{H}(\boldsymbol{x}, t) \text{ on } \Omega, \tag{8}$$

where $G_c$ represents the critical energy release rate (property of material), $\mathcal{H}(\boldsymbol{x}, t)$ is a local strain-history function, $\ell_0$ is the length scale parameter that controls the width of the diffusive region of the crack. The effect of $l_0$ has been verified by a series of numerical simulations [19, 18], demonstrating that the crack region has a larger width with an increasing $\ell_0$ while the phase field represents a sharp crack topology when $\ell_0 \to 0$. The phase field is used to smear out the crack surface over the domain $\Omega$. In the regularized model, correspondingly, the phase field must satisfy the following condition:

$$\phi(\boldsymbol{x}, t) = \begin{cases} 0 & \text{the material is intact,} \\ 1 & \text{the material is completely cracked.} \end{cases} \tag{9}$$

The local strain-history functional, $\mathcal{H}(\boldsymbol{x}, t)$ contains the maximum positive tensile energy, $\Psi_0^+$ in the history of deformation of the system [15] and is defined as:

$$\mathcal{H}(\boldsymbol{x}, t) = \max_{s \in [0, t]} \Psi_0^+(\boldsymbol{\epsilon}(\boldsymbol{x}, s)). \tag{10}$$

The strain-history function can also be used to initialize or nucleate the crack [14]. In particular, we set the initial strain-history function as [4]:

$$\mathcal{H}(\boldsymbol{x}, 0) = \begin{cases} \frac{BG_c}{2\ell_0}\left(1 - \frac{2d(\boldsymbol{x})}{\ell_0}\right) & \text{if } d(\boldsymbol{x}) \leq \frac{\ell_0}{2}, \\ 0 & \text{otherwise.} \end{cases} \tag{11}$$

4

where $d(\boldsymbol{x})$ is the distance from $\boldsymbol{x}$ to the crack tip, $B$ is a scalar parameter controlling the magnitude of the scalar history field and is computed as:

$$B(\phi) = \frac{1}{1 - \phi} \quad \text{for } \phi < 1. \tag{12}$$

The fracture energy, $\Psi_c$ of the newly formed cracks is expressed as:

$$\Psi_c = \int_\Omega \left( G_c \Gamma_n(\phi) + g(\phi)\mathcal{H}(\boldsymbol{x}, t) \right) \, d\Omega. \tag{13}$$

Here, $\Gamma_n(\phi)$ represents the crack density functional and $n$ is the order of the corresponding phase field model. For the second-order phase field model, $n = 2$, while for the fourth-order phase field model, $n = 4$. The fourth order phase model includes higher-order derivatives of $\phi$, leading to greater regularity in the exact solution of the phase field. In this case the cracked surface can be captured more accurately and fewer degrees of freedom are required to resolve the crack path relative to the second-order model. For the second and fourth order phase field model the crack density functionals, $\Gamma$ are defined as [3]:

$$
\begin{aligned}
\Gamma_2(\phi) &= \frac{1}{2\ell_0} \int_\Omega \left( \phi^2 + \frac{\ell_0^2}{2}|\nabla\phi|^2 \right) \, d\Omega, \\
\Gamma_4(\phi) &= \frac{1}{2\ell_0} \int_\Omega \left( \phi^2 + \frac{\ell_0^2}{2}|\nabla\phi|^2 + \frac{\ell_0^4}{16}|\Delta\phi|^2 \right) \, d\Omega.
\end{aligned}
\tag{14}
$$

In this work we study the growth of fracture employing the energy minimization approach. To that end, we solve the optimization problem defined as [5]:

$$
\begin{aligned}
\text{Minimize} \ &: \mathcal{E} = \Psi_e + \Psi_c, \\
\text{constrained to} \ &: \boldsymbol{u} = \bar{\boldsymbol{u}} \ \text{ on } \partial\Omega_D, \\
\text{such that} \ &: \Psi_e = \int_\Omega \left( g(\phi)\Psi_0^+ + \Psi_0^- \right) \, d\Omega, \\
&\quad \Psi_c = \int_\Omega G_c\Gamma_n + g(\phi)\mathcal{H}(\boldsymbol{x}, t) \, d\Omega.
\end{aligned}
\tag{15}
$$

The homogeneous Neumann boundary conditions are automatically satisfied when the variational energy principle is used.

## 2.2 Variational energy based neural networks

Suppose the computational domain $\Omega$ is partitioned into $p$ subdomains $\{\Omega_s : s = 1, 2\ldots, p\}$ such that $\Omega = \bigcup_{s=1}^p \Omega_s$. By partitioning, we imply that the division is non overlapping, and the subdomains intersect only on their common boundaries which is also called as *interface*. To simplify the discussion, consider the linear elastic problem defined in (4) as an example, where on a particular subdomain $\Omega_s$ we have:

$$-\nabla \cdot \boldsymbol{\sigma}_s(\boldsymbol{x}) = \boldsymbol{f}_s(\boldsymbol{x}) \ \text{ in } \Omega_s, \tag{16}$$

5

where $\boldsymbol{f}_s$ is the body force in the $s$-th subdomain, and $\boldsymbol{\sigma}_s$ is the Cauchy stress tensor associated with the material point in the $s$-th domain. Each subdomain is constrained by the continuity condition:

$$\boldsymbol{u}_i(\boldsymbol{x}) = \boldsymbol{u}_j(\boldsymbol{x}) \qquad \text{on } \Gamma_{ij}, \tag{17}$$

where $\Gamma_{ij}$ is the interface between the $i$-th and $j$-th subdomains, and $\boldsymbol{u}_i$ and $\boldsymbol{u}_j$ are the displacements on $\Omega_i$ and $\Omega_j$ respectively. The above boundary conditions also represent the interface transmission conditions between the neighbouring subdomains. For each of these subdomains, a separate deep neural network (DNN) is deployed.

A DNN [7], $\mathfrak{N}_{\mathrm{L}} : \mathbb{R}^d \mapsto \mathbb{R}^p$ is a non linear function defined as concatenations of affine maps with point-wise non linearities, in the form:

$$\mathfrak{N}_{\mathrm{L}}(\boldsymbol{x}) = \mathcal{W}_{\mathrm{L}} \tau_{\mathrm{L}} \left( \ldots \tau_3 \left( \mathcal{W}_2 \tau_2 \left( \mathcal{W}_1 \boldsymbol{x} + \beta_1 \right) + \beta_2 \right) \ldots \right) + \beta_{\mathrm{L}} \tag{18}$$

where, $\mathcal{W}_i$'s are weight matrices may not necessarily be square and $\beta_i$'s are referred as bias vectors. L is the depth (the number of layers) of the network and $\mathrm{L} \geq 3$. The input vector is $\boldsymbol{x}$ and the output vector of any arbitrary $\ell$-th layer is denoted by $\mathfrak{N}_\ell(\boldsymbol{x})$ in particular, $\mathfrak{N}_0(\boldsymbol{x}) = \boldsymbol{x}$. The non-linear monotonic function $\tau$ is known as activation function applied layer-wise to any vector, however the dimension of the input vector may vary depending on layers. However, regardless of input dimension, the activation function performs the same operations on all input entries. The activation function in the final layer is linear.

The primary goal of fracture mechanics is to determine the crack path. In this work, we have studied displacement-controlled fracture, *i.e.* this is growth of the crack by applying a displacement increment until failure. In addition, we assumed a constant displacement step, $\Delta u$. The neural network is trained and the strain-history function of each sub-domain is updated at each displacement increment in this configuration. In the beginning, the network parameters are initialized using a Gaussian distribution with Xavier initialization technique [8]. Let us first use a DNN to represent the displacement field, $\boldsymbol{U}_s$, and the phase-field, $\phi_s$ of the $s$-th subdomain, such that

$$(\boldsymbol{U}_s, \phi_s) = \mathfrak{N}_s \left( \boldsymbol{x}_s; [\mathcal{W}_s, \beta_s] \right). \tag{19}$$

Each subdomain is discretised into $n_e^s$ elements, and we generate the Gauss points within each element and their corresponding weights. The total variational energy is calculated at the Gauss points to approximate the integral. The displacements and the phase field at the common interfaces are assumed to be continuous. Therefore, for solving the PDE as a whole, we defining the loss function separately for the interior of each subdomain and the interfaces as follows:

$$\mathcal{L}_s^{int}(\mathcal{W}, \beta_s) = \Psi_e(\epsilon(U_s), \phi_s) + \Psi_c(G_c, \boldsymbol{x}_s)$$

$$\mathcal{L}_{ij}^{iface}(\mathcal{W}, \beta_s) = \frac{W_1}{N_{\Gamma_{ij}}} \sum_{k=1}^{N_{\Gamma_{ij}}} |\boldsymbol{u}_i(\boldsymbol{x}_k) - \boldsymbol{u}_j(\boldsymbol{x}_k)|^2$$

$$+ \frac{W_2}{N_{\Gamma_{ij}}} \sum_{k=1}^{N_{\Gamma_{ij}}} |\phi_i(\boldsymbol{x}_k) - \phi_j(\boldsymbol{x}_k)|^2$$

6

where $N_{\Gamma_s}$ represents the total training points scattered over its interfaces, respectively. The interface condition endowed with the loss function plays an important role for stitching the subdomains together. It ensures that the data information should propagate among the neighbouring domains. A sufficient number of collocation points needs to be generated on the interface leading to faster convergence of the algorithm. In (20), $W_i \forall \ i = 1, 2$ are penalizing parameters, which are chosen manually for balancing each of the loss terms and also for faster convergence. From the viewpoint of optimization it could be more sophisticated to multiply the constraints with suitable penalty coefficients. A method for adaptively choosing these penalty parameters has been proposed in [13].

# 3  Results

This numerical example is based on a unit square plate embedded with an eccentric hole, as shown in Figure 1(a). The bottom boundary remains fixed. At the top boundary, a quasi-static load is applied in the form of a prescribed displacement increment $\bar{u}$. The material properties considered for this problem are: $\lambda = 121.154$ kN/mm$^2$, $\mu = 80.77$ kN/mm$^2$, $G_c = 2.7 \times 10^3$ kN/mm. For this example, we have considered $l_0 = 0.02$. A displacement increment of $10^{-3}$ mm is applied at each incremental step.
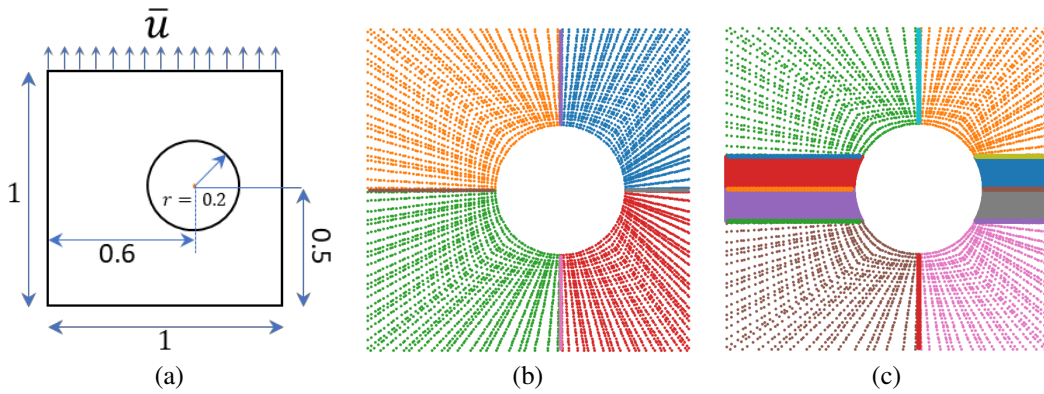


Figure 1: (a) Geometrical setup and boundary conditions for the square plate with eccentric hole test. All the units are in mm. (b) and (c) Distribution of training data over four and eight subdomains, respectively.

| # of domains | # elements per subdomain | Integration points per element | Interface points per subdomain |
|---|---|---|---|
| 4 | $12^2$ | 4 | 1600 |
| 8 | $8^2, 14^2$ | 4 | 1000 |

Table 1: Summary of the subdomain arrangements studied in the numerical example.
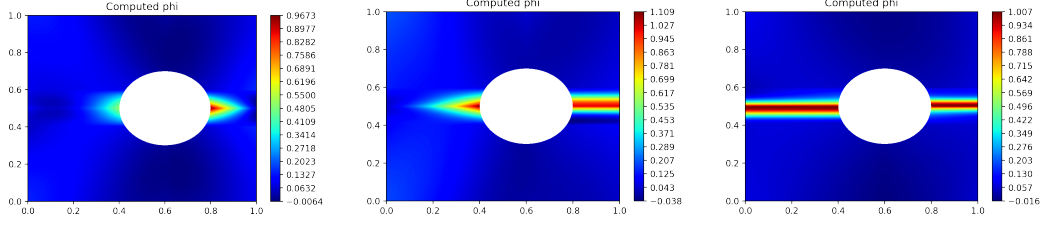
7

Figure 2: Crack growth in the square plate with eccentric hole, using the fourth-order phase field model and $8$ subdomains.
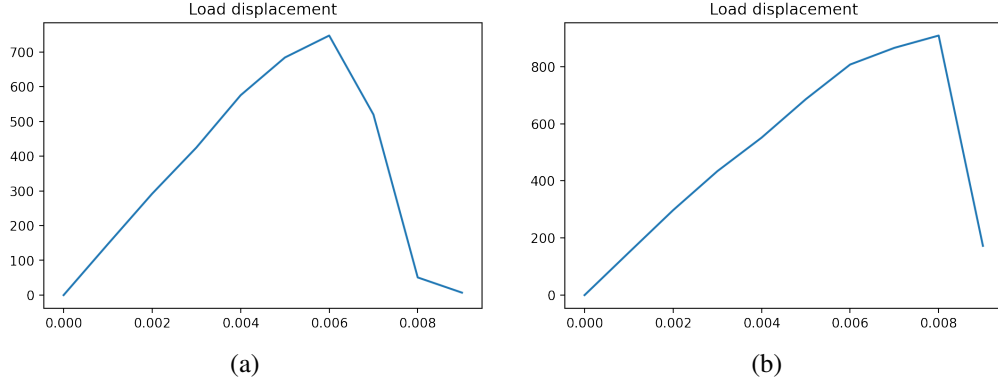


Figure 3: Load displacement plots of square plate with eccentric hole. (a) $4$ subdomains, and (b) $8$ subdomains.

In Table 1, the details of the experimental setup of $4$ and $8$ subdomains are provided. A $3$-layers fully-connected neural networks with $50$ neurons per hidden layer with $swish$ activation is employed. The final layer uses linear activation function. The outputs for the elastic field are altered to exactly match the Dirichlet boundary conditions, as follows:

$$
\begin{aligned}
\boldsymbol{u} &= x\boldsymbol{u}_\theta, \\
\boldsymbol{v} &= y(y-1)\boldsymbol{v}_\theta + y\Delta u,
\end{aligned}
\tag{20}
$$

where $\boldsymbol{u}$ and $\boldsymbol{v}$ are the solutions of the elastic field in coordinate axes, and $\boldsymbol{u}_\theta$ and $\boldsymbol{v}_\theta$ are the neural network approximations of the displacement field in $x-$ and $y-$ axes. Figure 2 demonstrates the results of the fourth-order phase-field model obtained using the proposed approach. The load-displacement curves for both the experiments are shown in Figure 3. In the specimen $8$ subdomains, we observe a sharper drop-off in the load compared to the experiment with $4$ subdomains.

# 4   Conclusion

In this work, we have proposed a domain decomposition approach for deep energy method, that aims to accurately resolve the crack path employing the phase field mod-

8

eling approach. The proposed approach is more efficient and accurate than its predecessor [9, 10]. The proposed method can be used to solve any differential equation in its weak form. This is accomplished by enforcing the residual continuity requirement along the shared subdomain interfaces. For the numerical examples, we observe that the results obtained using the proposed approach match closely with results from the literature.

# References

[1] A. Griffith. The Phenomena of Rupture and Flow in Solids. *Philosophical Transactions of the Royal Society of London*, 221(Series A):163–198, 1921.

[2] H. Amor, J.-J. Marigo, and C. Maurini. Regularized formulation of the variational brittle fracture with unilateral contact: Numerical experiments. *Journal of the Mechanics and Physics of Solids*, 57(8):1209–1229, 2009.

[3] M. J. Borden, T. J. Hughes, C. M. Landis, and C. V. Verhoosel. A higher-order phase-field model for brittle fracture: Formulation and analysis within the isogeometric analysis framework. *Computer Methods in Applied Mechanics and Engineering*, 273:100–118, 2014.

[4] M. J. Borden, C. V. Verhoosel, M. A. Scott, T. J. Hughes, and C. M. Landis. A phase-field description of dynamic brittle fracture. *Computer Methods in Applied Mechanics and Engineering*, 217-220:77–95, apr 2012.

[5] B. Bourdin, G. Francfort, and J.-J. Marigo. Numerical experiments in revisited brittle fracture. *Journal of the Mechanics and Physics of Solids*, 48(4):797–826, apr 2000.

[6] B. Bourdin, C. J. Larsen, and C. L. Richardson. A time-discrete model for dynamic fracture based on crack regularization. *International journal of fracture*, 168(2):133–143, 2011.

[7] A. Chakraborty, T. Wick, X. Zhuang, and T. Rabczuk. Multigoal-oriented dual-weighted-residual error estimation using deep neural networks. *arXiv e-prints*, pages arXiv–2112, 2021.

[8] X. Glorot and Y. Bengio. Understanding the difficulty of training deep feedforward neural networks. In *Proceedings of the thirteenth international conference on artificial intelligence and statistics*, pages 249–256. JMLR Workshop and Conference Proceedings, 2010.

[9] S. Goswami, C. Anitescu, S. Chakraborty, and T. Rabczuk. Transfer learning enhanced physics informed neural network for phase-field modeling of fracture. *Theoretical and Applied Fracture Mechanics*, 106:102447, 2020.

[10] S. Goswami, C. Anitescu, and T. Rabczuk. Adaptive fourth-order phase field analysis using deep energy minimization. *Theoretical and Applied Fracture Mechanics*, 107:102527, 2020.

[11] I. E. Lagaris, A. Likas, and D. I. Fotiadis. Artificial neural networks for solving ordinary and partial differential equations. *IEEE transactions on neural networks*, 9(5):987–1000, 1998.

[12] H. Lee and I. S. Kang. Neural algorithm for solving differential equations. *Journal of Computational Physics*, 91(1):110–131, 1990.

[13] L. McClenny and U. Braga-Neto. Self-adaptive physics-informed neural networks using a soft attention mechanism. *arXiv preprint arXiv:2009.04544*, 2020.

[14] C. Miehe, M. Hofacker, and F. Welschinger. A phase field model for rate-independent crack propagation: Robust algorithmic implementation based on operator splits. *Computer Methods in Applied Mechanics and Engineering*, 199(45-48):2765–2778, 2010.

[15] C. Miehe, F. Welschinger, and M. Hofacker. Thermodynamically consistent phase-field models of fracture: Variational principles and multi-field fe implementations. *International journal for numerical methods in engineering*, 83(10):1273–1311, 2010.

[16] M. Raissi, P. Perdikaris, and G. E. Karniadakis. Physics-informed neural networks: A deep learning framework for solving forward and inverse problems involving nonlinear partial differential equations. *Journal of Computational Physics*, 378:686–707, 2019.

[17] E. Samaniego, C. Anitescu, S. Goswami, V. M. Nguyen-Thanh, H. Guo, K. Hamdia, X. Zhuang, and T. Rabczuk. An energy approach to the solution of partial differential equations in computational mechanics via machine learning: Concepts, implementation and applications. *Computer Methods in Applied Mechanics and Engineering*, 362:112790, 2020.

[18] S. Zhou, T. Rabczuk, and X. Zhuang. Phase field modeling of quasi-static and dynamic crack propagation: Comsol implementation and case studies. *Advances in Engineering Software*, 122:31–49, 2018.

[19] S. Zhou, X. Zhuang, H. Zhu, and T. Rabczuk. Phase field modelling of crack propagation, branching and coalescence in rocks. *Theoretical and Applied Fracture Mechanics*, 96:174–192, 2018.